

# Deep hydration: Poly(ethylene glycol) $M_w$ 2000–8000 Da probed by vibrational spectrometry and small-angle neutron scattering and assignment of $\Delta G^\circ$ to individual water layers

Kenneth A. Rubinson<sup>a,b,\*</sup>, Curtis W. Meuse<sup>a</sup>

<sup>a</sup> National Institute of Standards and Technology, Gaithersburg, MD 20899, USA

<sup>b</sup> Department of Biochemistry and Molecular Biology, Wright State University, Dayton, OH 45435, USA

## ARTICLE INFO

### Article history:

Received 6 September 2012

Received in revised form

28 October 2012

Accepted 2 November 2012

Available online 23 November 2012

### Keywords:

SANS

Poly(ethylene glycol)

Water structure

## ABSTRACT

Aqueous solutions of poly(ethylene glycol) (PEG) exhibit some remarkable properties, among which is the small changes in water activity compared to the volumes occupied by the PEG: For example, the water in a 20% mass fraction solution of 6000 Da PEG has an activity of 0.9939. We have investigated PEGs with molecular weights 200, 400, 1000, 2000, 4000, and 8000 Da in the concentration range 1% to 17% mass fraction at neutral pH and with added KCl concentrations of 10 mmol L<sup>-1</sup> in aqueous solutions—conditions near those for promoting protein crystallization. These solutions exhibit a structural change at around 6% mass fraction as seen in the solution viscosities, compressibilities, and infrared spectra. Raman spectroscopy shows that the PEGs remain in the same structural form over the concentration range, and the infrared spectra indicate that the change must be due to a local shift in the water structure. Modeling of the results from small-angle neutron scattering (SANS) on the solutions suggests that the structures of the PEGs in the molecular mass range 2000 Da to 8000 Da are paired in the solution, and the separation distance decreases with increasing PEG concentration. From the structure, it becomes clear that the small effect on water activity occurs because of screening by the more weakly bound outer layers. From the bulk measurement of  $a_w$  and with reasonable assumptions, a free energy  $\Delta G^\circ$  can be assigned to each of the fourth, third, and second hydration layers.

© 2012 Elsevier Ltd. All rights reserved.

## 1. Introduction

Water solutions of poly(ethylene glycol) (PEG) exhibit some remarkable properties, among which are exceptionally small changes in water activity  $a_w$  compared to the volumes occupied by the PEG. For example, as measured by Großmann [1] in a 67.5% mass fraction solution of PEG 6000, where approximately two-thirds of the water has been displaced by 6000 Da PEG,  $a_w = 0.8919$ , and a 20% w/w solution has a water activity of 0.9939, only 0.0061 less than the pure solvent. However, despite apparently not perturbing the water properties, PEG in solutions are effective in promoting crystallizations of proteins, the application that has motivated this study.

*Abbreviations:* PEG, Poly(ethylene glycol); SANS, small-angle neutron scattering; ATR, attenuated total reflection; AFM, atomic force microscopy; IR, infrared; EO, ethylene oxide (monomer component of PEG).

\* Corresponding author. National Institute of Standards and Technology, Gaithersburg, MD 20899, USA.

E-mail addresses: [Rubinson@nist.gov](mailto:Rubinson@nist.gov), [kenneth.rubinson@wright.edu](mailto:kenneth.rubinson@wright.edu) (K.A. Rubinson), [Curtis.Meuse@nist.gov](mailto:Curtis.Meuse@nist.gov) (C.W. Meuse).

We have investigated PEGs with molecular weights 200, 400, 1000, 2000, 4000, and 8000 Da in the concentration range 1% by weight to 17% by weight at neutral pH and with KCl concentrations around 10 mM (mM = mmol L<sup>-1</sup>) in aqueous solutions – at the low end of the usual ionic strengths. In general the PEGs used effectively for crystallization are those between 1000 Da and 8000 Da, and the facts collected in this work indicate that this range of molecular weights do, indeed, comprise a unique group.

Prior work has shown that numerous properties of the PEG solutions have a break in their trends with concentration at around 6%. The breaks occur in the concentration dependencies of the viscosity [2] and compressibility [2,3]. Here, we find a break in infrared spectral absorbances, while the Raman spectra do not show a similar break in relative emission. Characterizing the structure change that causes this break in the trends with concentration is the subject of this paper.

Modeling of the results from small-angle neutron scattering (SANS) of the higher molecular mass PEGs—PEG 2000, 4000, and 8000—has suggested that these molecules reside in the form of sheets [4]. This conclusion arises from the measured radius of

gyration depending on the square root of the mass, the sizes of the structures giving a consistent stoichiometry, and the observation that the scattering is characteristic of independent particles under conditions where Gaussian or even compressed coils would overlap. Further, similar structures are seen for ethanol.

Here, we show that these sheets come closer together as the polymer:water ratio increases, and that this observation can be related to phenomena such as the fixed spacing between bilayers in multilayer liposomes [5,6]. As will be shown, the length scale of the solution structures is important, and, with a number of straightforward assumptions together with the experimentally measured activity of water by Großmann et al. [1], each layer of hydrating waters can be assigned an approximate  $\Delta G^\circ$ .

## 2. Materials and methods<sup>1</sup>

### 2.1. Poly(ethylene glycol) solutions

PEGs with average molecular masses of 1000 Da, 2000 Da, 4000 Da, and 8000 Da are interchangeably listed as PEG 1000 or PEG 1k, and so forth. The following PEGs were used (source, lot number, initial pD of 50% g/mL solutions): PEG 400 (Hampton Research, Lot 260-323, 6.0); PEG 1000 (Sigma, Lot 12K0126, 3.2); PEG 2000 (Fluka, Lot 35387011, 8.1); PEG 4000 (Fluka, Lot 35264911, 7.6); PEG 8000 (Aldrich, Lot 09626HN, 9.8). The stock solutions were brought to  $\approx$ pD 7 with concentrated sodium deuteroxide or  $d_4$ -acetic acid. To form the final solutions the appropriate amounts of stock 1.0 M ( $M = \text{mol L}^{-1}$ ) potassium phosphate buffer pD 6.8, 10%  $\text{NaN}_3$ , and 4 M KCl were added to each sample. The final  $\text{D}_2\text{O}$  solutions had, besides the PEGs, 10 mM added KCl, 0.1%  $\text{NaN}_3$ , and 10 mM phosphate buffer with final pDs between 6.5 and 7.7. The pD values were those recorded by a glass electrode standardized in  $\text{H}_2\text{O}$ . No isotope correction was made with the assumption that the unmodified value was more correct since it is likely that the buffer pD and electrode surface's  $\text{pK}_a$  shifted approximately the same amount with the level of D-H substitution. All PEG and salt concentrations lie well below those that produce two-phase systems [7]. Keeping the pH/pD near neutral minimizes proton binding to the PEGs while also minimizing possible hydrolysis. The buffer and KCl have been added to keep the total ionic strength approximately constant since some level of ionic impurities of unknown identity [8] seem to exist in the six different PEGs. They do not form neutral solutions upon addition to water. In other words, these solutions have been made as constant in their solution conditions as possible consistent with minimizing materials other than the PEGs and water.

The effect of KCl in the solution on the PEGs is expected to be minimal because its concentration is low compared to binding constant and because its quantity is small compared to the EO content of the solutions. Both are explained further next. In water, potassium binds to its best binding crown ether 18-crown-6 with  $\log K_f = 2$  as found by a number of groups [9–11]. This means that for the 18-crown-6, half of the 10 mM  $\text{K}^+$  will be bound at 15 mM of the crown. However, for open-chain complexing agents, binding constants tend to be reduced by a factor of  $10^2$  to  $10^4$  fold [12,13]. Even for the smallest change in ratio of 100, we expect binding constants in the molar range. For example, with a formation

constant of 1 M, the 10 mM  $\text{K}^+$  would bind to 0.5% of the PEG molecules.

Further, the quantity of  $\text{K}^+$  present cannot control the structure of the PEGs because even the lowest concentration of PEG at 1% is more than 200 mM in monomer. Any unexpectedly (never observed) strong binding of  $\text{K}^+$  in a structure the same as 18-crown-6 would occupy less than 30% of the PEGs structure. Again, assuming a strong binding that has never been observed, in the most concentrated solutions, all the  $\text{K}^+$  would be taken up by 2% of the PEG, which would have no observable effect on the scattering from the 98% not associated.

### 2.2. Calculation of PEG concentrations

Three very different ranges of measured PEG partial densities are found by experiment. First, from the lack of contrast in x-ray scattering from an aqueous PEG solution, the water-equivalent electron density gives a physical density for PEG of  $1.02 \text{ g cm}^{-3}$  [7]. Second, Sandell & Goring [14] found by dilatometry that the density of PEG 1k is temperature dependent. Fitting equations show the density varying from 1.13 at 25 °C to 1.20 at 10 °C. A third, and quite different range at 25 °C was found by Lepori & Mellica [15]. Assuming the condition that the water has its bulk density at 25 °C of 0.99705 uniformly throughout, they find that PEG 1k and PEG 2k both have density 1.19 in the solution and that this value holds from PEG 1k to PEG 15k. We found nearly the same value using the 25 °C data from Cruz et al. [16,17] for PEG 3k and PEG 6k for concentrations below 15% mass fraction of the solution. Using the same assumption of a uniform water phase and the PEG residing in it, the calculation yields an additive density for the PEGs of  $1.20 \text{ g cm}^{-3}$ . We choose to use the value of 1.20 for the partial density of PEG in aqueous solution for all the molecular masses measured here. Attributing the density and especially the temperature dependence specifically to the PEG or to the water cannot be done without as yet unprovable assumptions.

Since our data in  $\text{D}_2\text{O}$  is to be compared to literature measurements mostly carried out in  $\text{H}_2\text{O}$ , the mass percent of PEG in the solutions was initially calculated from a mass-to-volume measurement. The mass percent values have been calculated as if the solvent were  $\text{H}_2\text{O}$  instead of  $\text{D}_2\text{O}$ . Our concentrations can, then, be directly compared to the many other measurements reported in the literature and noted in the text.

*Infrared Spectra:* The attenuated total reflection spectra were obtained using a Bruker Equinox 55 spectrometer (Billerica, MA) with a VeeMax external reflection accessory (Pike Technologies, Madison, WI) with a ZnSe 45° total internal reflection crystal. The spectra were the average of two scans ( $4 \text{ cm}^{-1}$  resolution, 2 min each) corrected for background including water vapor with Bruker's Opus software version 5.5. Further data fitting, data manipulation, and wavenumber and absorbance measurement were also performed with Bruker's Opus software. Display graphs were produced with Igor (WaveMetrics, Portland, OR) from the ascii files of the spectra.

Several polarized spectra were collected at different PEG molecular weights and concentrations to determine if any of the observed changes might be related to PEG interactions with the ATR crystal surfaces. These spectra revealed no indication of surface induced orientation, which leaves all changes to be explained by solution-based mechanisms.

Since neither the line widths nor line shapes shifted with concentration, the peak heights were used to measure change in absorbance. The linearities of the line segments fitting absorbance over the concentration range suggest that any changes in baseline can be ignored except at the transition for the PEG 8000 solution, which, since it is unique, is not included in the discussion.

<sup>1</sup> (Disclaimer): Certain trade names and company products are identified in order to specify adequately the procedure. In no case does such identification imply recommendation or endorsement by the National Institute of Standards and Technology, nor does it imply that the products are necessarily the best for the purpose.

Changes in the spectra might be caused by dielectric constant differences. However, in solutions of ethanol, these differences have been shown to be small enough to ignore here [18]. As a result, we discount dielectric changes in the discussion.

### 2.3. Raman spectra

The Raman spectra were obtained at 90° scattering on a Bruker RFS-100 Fourier-transform Raman spectrometer (Billerica, MA) with a 1064 nm laser line (diode-pumped CW Nd-YAG laser) at 900 mW power and 4 cm<sup>-1</sup> resolution with 256 scans averaged for each spectrum collected in the range 4000 cm<sup>-1</sup> to 1000 cm<sup>-1</sup> Raman shift. A liquid-nitrogen-cooled Ge diode was used for detection. The acquired interferograms were apodized with a Blackman-Harris four-point filter and zero-filled by a factor of 4 prior to transformation.

### 2.4. SANS data collection

SANS from solutions of PEGs in D<sub>2</sub>O (Cambridge Isotope Laboratories) were held in 2 mm pathlength cylindrical silica spectrometry cells (volume ~640 μL). SANS measurements were performed on the NG7 and NG3 30 m SANS instruments at the NIST Center for Neutron Research (NCNR) in Gaithersburg, MD [86]. The PEG samples were measured λ = 5.2 Å or 6 Å with Δλ/λ = 0.11. Scattered neutrons were detected with a 64 cm × 64 cm two-dimensional position sensitive detector with (128 × 128) pixels and 0.5 cm resolution per pixel. Data reduction was accomplished using Igor Pro software (WaveMetrics, Lake Oswego, OR) with SANS macros developed at the NCNR [87]. Raw counts were normalized to a common monitor count and corrected for empty cell counts, ambient room background counts, and non-uniform detector response. Data were placed on an absolute scale by normalizing the scattering intensity to the incident beam flux for each individual pixel. The data were placed on an absolute scale through calibrating against scattering from a silica gel standard. Finally, the data were radially averaged to produce the scattering intensity *I*(*q*) to plot as *I*(*q*) versus *q* curves— where *q* = (4π/λ)sin θ—with 2θ the scattering angle measured from the axis of the incoming neutron beam. Sample-to-detector positions used were either 1.5 m or 1.3 m, which provides a *q* range from 0.03 Å<sup>-1</sup> to 0.45 Å<sup>-1</sup> equal to a length range of ~200 Å to 14 Å.

### 2.5. Nonparametric calculations of experimental *S*(*q*) curves

In practice, the scattering that is measured from macromolecules in solution *I*(*q*) includes contributions from the form (intramolecular shape) factor, *P*(*q*), and the interparticle structure factor, *S*(*q*), as well as background scattering from solvents, buffers and cuvettes. The contributions to the measured scattering intensity *I*(*q*) are related by:

$$I(q) = nV^2(\Delta\rho)^2P(q)S(q) + B(q) \quad (1)$$

The units of the scattering are inverse length (cm<sup>-1</sup>), and *B*(*q*) is the total background to be subtracted. Also, (Δρ)<sup>2</sup> is the contrast in scattering between the PEGs and the solvent, *n* the number density of scatterers, and *V* is the volume of the individual scatterers. Here, the *B*(*q*) consists of separately measured buffer scattering as well as the inelastic scattering contribution expected from the hydrogens at each PEG concentration [3]. Both were subtracted to obtain the corrected *I*(*q*).

The form factor *P*(*q*) was separated from the interparticle structure factor *S*(*q*) by obtaining the scattering curves at two different concentrations; call them 1 and 2. However, for scatterers

that do not change shape with concentration (assumed for the PEGs within the concentration range reported here), and with the variable *n* reflecting the concentration, only the terms *I*(*q*) and *S*(*q*) vary. With properly subtracted background, we assume the lowest concentration measured the molecules are independent and exhibit no correlated structure, i.e., they are noninteracting. Then, *S*(*q*)<sub>low</sub> = 1, and the *S*(*q*) curves for higher concentrations are found from

$$S(q)_{\text{interacting}} = \frac{n_{\text{noninteracting}}}{n_{\text{interacting}}} \frac{I(q)_{\text{interacting}}}{I(q)_{\text{noninteracting}}} \quad (2)$$

In this way *S*(*q*) can be found from the scattering data without requiring a model structure. As shown by Hayter & Penfold (1983), this separation of *P*(*q*) and *S*(*q*) strictly holds only for homogeneous monodisperse spheres in solution but has been found to work for nonspherical solutes that are not monodisperse. This may be due to the independent, noninteracting molecules' scattering being rotationally (spherically) averaged over the time scale of the experiment. An inherent assumption of the quality of this separation is the unchanging shape of the scatterer with concentration.

The values of *S*(0) were found by short, smooth extensions of the *S*(*q*) graph to *q* = 0. We estimate the *S*(0) values have relative uncertainties of less than 5%, and within that range were insensitive to the method of extrapolation.

### 2.6. Modeling of the *S*(*q*) curves

Simulation was done by the method of Heidorn [19] where a set of spheres is substituted within the volume of the scattering structure. Here, the PEGs are simulated with a set of uniform spheres of 4Å diameter in a rigid, flat, rectangular array the size of the PEGs. The PEG sizes used were: PEG 2k, (20 × 40) Å; PEG 4k, (28 × 78) Å; PEG 8k, (42 × 100) Å [4]. Two of these rigid plates were set at different fixed distances apart. The scattering curve for the intermolecular structure was calculated using the formula developed by Debye for scattering by scattering spherical pairs randomly oriented in solution [20] but summing only for pairs of spheres not in the same sheet. This calculation provides an approximate intermolecular *I*(*q*), which was converted to fit the experimental *S*(*q*) data by inverting the summed scattering curve followed by scaling and adding an appropriate constant background. This transformation is based on the relationship [21]

$$S(q) - 1 = 4\pi\phi \int_0^\infty [g(r) - 1] \frac{\text{Sin}(qr)}{qr} r^2 dr \quad (3)$$

where φ is the neutron flux, and *g*(*r*) is the correlation coefficient between the structural elements. If the correlation is unity, then it yields a fixed intermolecular structure rotationally averaged. This approximation was judged to be adequate to find the relationship between the observed peaks of the *S*(*q*) curves and the true separations of the assumed rigid PEG sheets at the different concentrations. Even though the peaks are fit to find a pair separation, the calculated curves are not expected to be correct over the full *q* range if the assumption of two isolated, paired sheets is incorrect and when the sheets are not rigid.

A simulation for three stacked sheets was also made. As expected, the diffraction sharpened but did not fit as well to the data. However, higher multiple stacking cannot be eliminated as a possibility since reduced ordering in the structure for which we see evidence in the two-plate fits would have two effects. One is that the coherence across two spaces be lowered such that only the adjacent pairs appear from among the stack. The second is that the

multi-plate scattering is smeared so that it has little influence on the broad two-plate scatter that appears.

### 2.7. Treatment of data values taken from the literature

Published data sets that are shown were taken either from tables or from graphs digitized with Un-Scan-It (Silk Scientific, Orem, UT). In converting various concentration units to a common one, the PEGs added to aqueous solutions was assumed to exhibit a macroscopic partial density of 1.20 as described above.

## 3. Results and discussion

### 3.1. PEG solution properties

Aqueous solutions of poly(ethylene glycol)s, PEGs, have long been popular objects of investigations of water soluble polymers. The results of such studies appear in many cases to be contradictory with others, and we find that is not surprising since the properties of the solutions often differ depending on the average mass of the oligomer or polymer as well as the concentration of each and other properties such as the concentrations and identities of added salts. Data from the literature has been selected to illustrate these changes that our vibrational spectral data and scattering data further clarify. The graphs illustrate changes that we have chosen to fit with regression line segments. Some of the sets of data might conceivably be fit with curved lines, but, taken together, the data argues for breaks in the properties that occur over relatively narrow ranges of molecular weights and concentrations. After an introduction to the differences in solution properties with molecular weight and concentration, a more extensive discussion about the vibrational spectroscopy and neutron scattering follows.

### 3.2. The differences in solution properties with molecular mass

Fig. 1 shows a log–log graph of the apparent specific volumes at infinite dilution at 25.0 °C for PEGs over a range of molecular weights as found by Kirinčić & Klofutur [22]. The molecular masses are those of the samples determined by viscometry and are all greater than the nominal masses by as much as 35%. A break in the trend with increasing molecular weights occurs around mass 1000.

Fig. 2 shows a log–log graph of Kirinčić & Klofutur's tabulated intrinsic viscosities of PEGs in aqueous solutions at 25.0 °C versus their nominal molecular weights [23]. These values further support

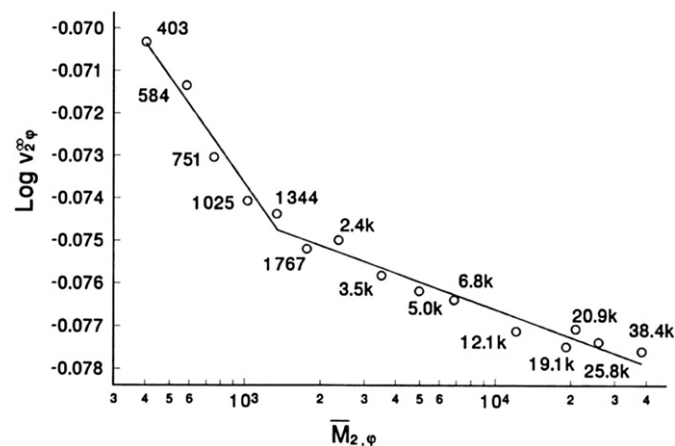


Fig. 1. Log–log plot of the apparent specific volumes of the solute at infinite dilution of PEGs in water at 25 °C versus the molecular mass. These values were determined by Kirinčić and Klofutur [22].

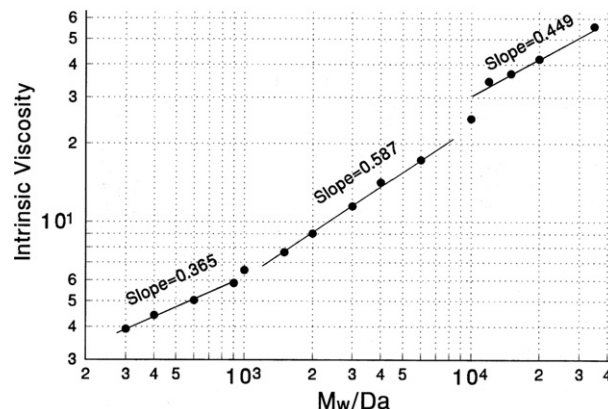


Fig. 2. Log–log plot of the intrinsic viscosities over a range of molecular masses of PEGs in water at 25 °C. The values are taken from the work of Kirinčić and Klofutur [23].

a change in solution structure around the same 1000 Da molecular weight range. Here, three different regions appear as indicated by the slopes of the sets of points; the two that lie between regions apparently do not belong with those on either side. Again, a break occurs around PEG 1000. However, a second break appears at PEG 10k, which is beyond the molecular weight range measured in this work. As will be shown, PEG 8k has properties quite different from the other PEGs with masses between 1000 and 4000. It may lie in the upper gap under these conditions as well.

Our infrared data from the PEGs, as shown in Fig. 3, corroborates the significant structural difference that occurs around molecular mass 1000. If we assume that the absorbances of the various bands reflect the populations of local conformations of the molecules, then the changes in the spectra with molecular mass, indicate that the structures become confined into fewer forms with the break about molecular mass 1000, above which the bands are nearly coincident. That is, the clearly separate bands between 870  $\text{cm}^{-1}$

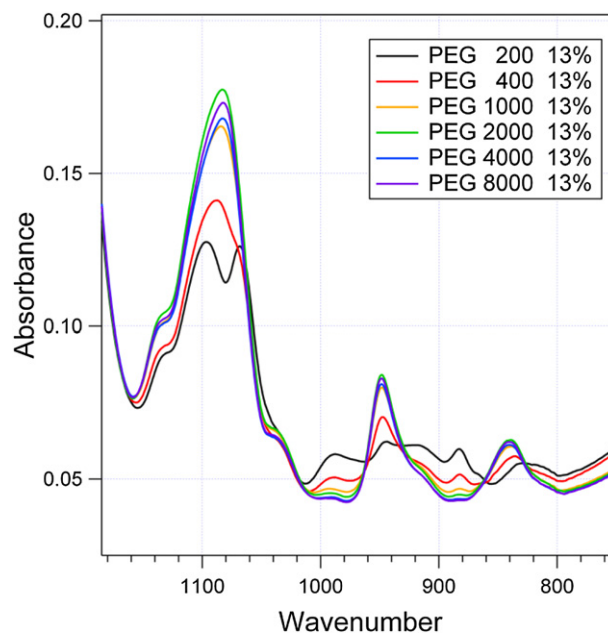


Fig. 3. The infrared spectra of PEG solutions of 13 weight percent with various molecular weights in  $\text{D}_2\text{O}$ , 99.9% d with 100 mM KCl added and buffered near neutral pH.

and  $1050\text{ cm}^{-1}$  coalesce into one narrower band indicative of a more ordered structure. (Complete data sets of the infrared spectra are included in the [Supplementary material](#).) All three of these sets of measurements—as shown in [Figs. 1–3](#)—indicate differences in the structures in aqueous PEG solutions as they depend on the PEG molecular mass.

### 3.3. Changes in solution properties with concentration

The viscosities of aqueous PEG 6000 solutions were measured over the appropriate range of concentrations by Kalyanasundaram et al. [2] Their data is replotted in [Fig. 4](#) after converting the published values into our customary units. Over the range, the data falls along two regression line segments with a slope ratio of 2.4 at  $30\text{ }^\circ\text{C}$ . However, a clear break does not occur at higher temperatures. In the same graph, the measured solution viscosity for PEG 4000 at  $25\text{ }^\circ\text{C}$  from Kirinčić and Klofutar [23] is also shown. However, solutions of lower molecular weight PEGs do not show a clear break between the slopes of two regression line segments. Our data from neutron scattering and vibrational spectroscopy allow us to expand on these published results and to explain the causes of this trend break.

In [Fig. 5](#) is shown data from two different measurement methods for the compressibilities of PEG solutions. At the top is plotted the compressibility for a PEG 6000 solution relative to pure water obtained by Kalyanasundaram et al. [2] with ultrasonic interferometry. The results differ greatly from those determined by small-angle neutron scattering (SANS) shown below it [3]. The SANS values plotted are obtained from the part of the neutron scattering that arises from the intermolecular structure of the solutes in solution. This plot of the scattering versus  $q$  is labeled  $S(q)$ , where  $q = (4\pi/\lambda) \sin \theta$ , with  $\lambda$  the deBroglie wavelength of the neutrons and  $2\theta$  the angle at which the scattering is measured. The value  $S(0)$  – the value of  $S(q)$  extrapolated to  $q = 0$  – for the

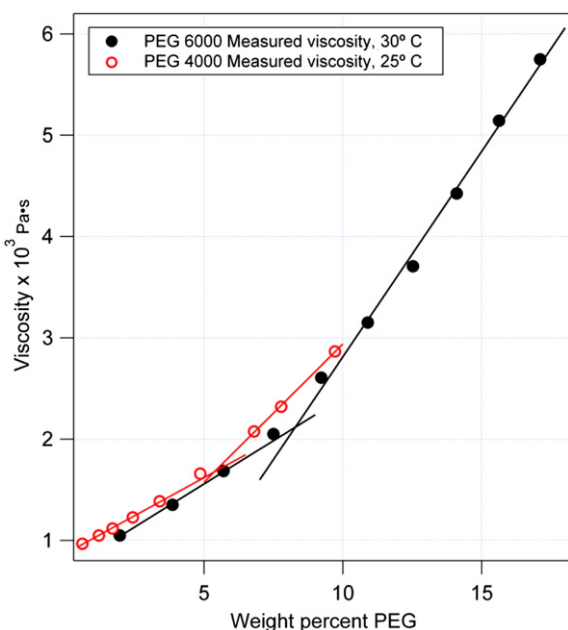


**Fig. 4.** Measured PEG aqueous solution viscosities. Data for PEG 6000 is taken from Kalyanasundaram [2] At higher temperatures, the break disappears. Data for PEG 4000 is taken from Kirinčić and Klofutar. [23] Within the concentration ranges measured, solutions of lower molecular weight PEGs did not show a clear break. The PEG 6000 data also could be fit by a power function  $\eta = 0.963 + 0.0329(\text{weight } \%)^{1.76}$  with  $r^2 = 0.999$ .

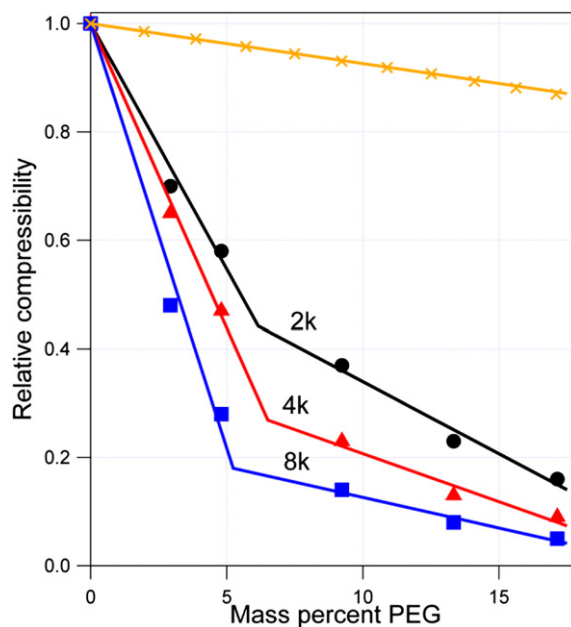


**Fig. 5.** Relative compressibilities of PEG solutions. The top line is the data from ultrasonic interferometry for PEG 6000 in water as determined by Kalyanasundaram et al. [2]. The bottom three plots are the values for PEG 2000, 4000, and 8000 in  $\text{D}_2\text{O}$  solutions as measured by SANS and described in a previous work [3].

oligomer solution's scattering can be related to the isothermal compressibility of the solution by  $S(0) = n_p k_B T \chi_T$ , where  $n_p$  is the number of particles and  $\chi_T$  the compressibility [24]. The value  $S(0) = 1$  is the relative compressibility for the solvent alone.

This simple equation relating  $S(0)$  to the compressibility is derived for an atomic fluid, which does not characterize a PEG solution. The solution compressibilities found from  $S(0)$  in SANS are in essence the spatial correlations (consider indistinct structures: more blurry means a lower structural correlation) between the scattering particles where the particles themselves serve as probes for the compressibility they experience with their  $k_B T$ -induced motions. The lower the compressibility, the lower the displacements by thermal motion. The majority of scattering here arises from the contrast between the PEG's protons and the  $\text{D}_2\text{O}$  solvent, and these protons are bound to the molecular backbone. The value of  $S(0)$  represents the range of displacements that these protons can occupy, where the lower the  $S(0)$  value represent smaller displacements. In other words, the main scatterers, the protons on the PEGs, are restrained more the lower the solution compressibility. As a result, the measurement of compressibility with SANS differs from those using ultrasound or other bulk measurements in which the measurement reflects changes in both the polymer and the water structures. This is the cause of the divergence so clearly seen in the graph. An analysis beyond describing this general difference in origins of the measurements is outside of the scope of this work, however.

Infrared spectra also exhibit a discontinuity of absorbance with concentration as shown in [Fig. 6](#) by a few representative bands for  $\text{D}_2\text{O}$  solutions of PEG 2000. Here are plotted the measured peak absorbances as they change with PEG concentration. The ratio of the molar absorptivity at the higher concentration range compared to the lower range is around 1.6.

Finally, in this overview of the measurements, the water activity in solutions with PEGs as solutes remains high even when the oligomers or polymers comprise a large volume fraction of the solution. The data of Großmann [1] for PEG 6000 shows this and is

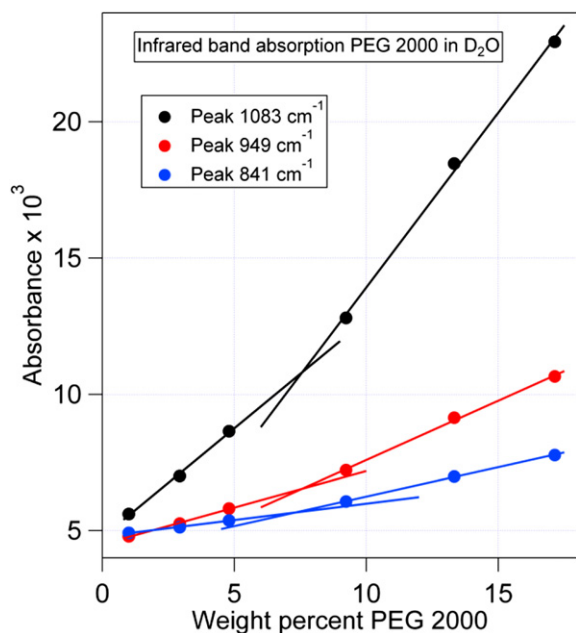


Fig. 6. Absorbances of selected IR bands for PEG 2000 over the concentration range probed in this work.

plotted in two ways in Fig. 7. In Fig. 7a, the measured  $a_w$  at 293.15 K for PEG 6000 is plotted with a best fit line. The concentration range shown is nearly twice our experimental range for the IR and SANS. The graph in Fig. 7b shows that the free energy of the water – represented by the logarithm of the experimental  $a_w$  – changes with PEG concentration with the power 2.8. In the remainder of this section, we characterize the nature of the transitions described above and seek to connect PEG concentrations with structural distances and subsequently to the free energies of the layers of hydration. In so doing, we can explain why the water activity changes are so small.

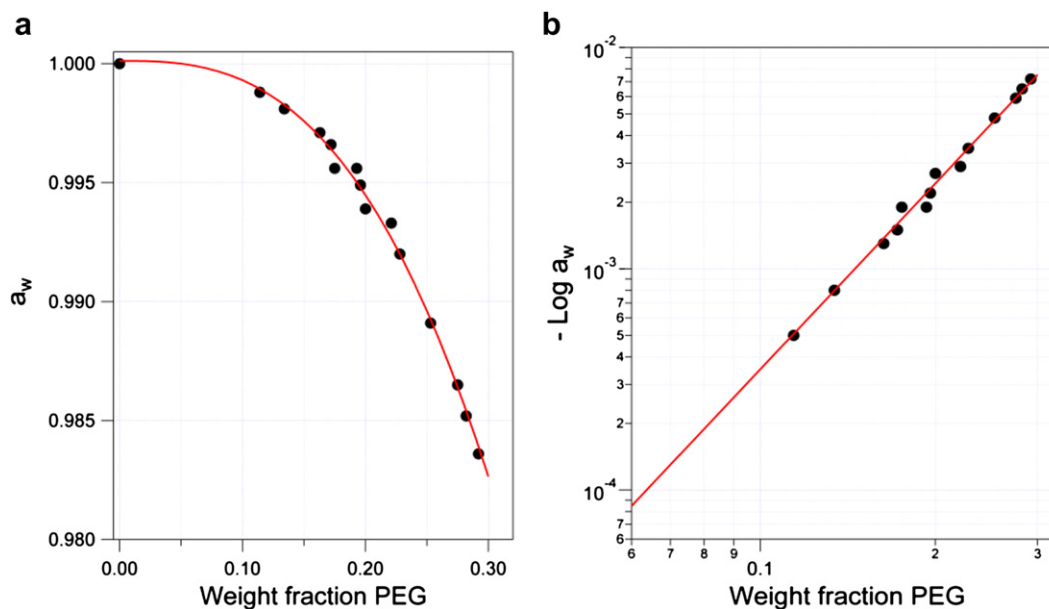


Fig. 7. a) Cartesian plot of the measured water activity versus percent weight of PEG 6000. The data is from Großmann [1]. b) A replot of the data as proportional to free energy by taking the logarithm of  $a_w$  and using a log–log format. The equation for fitting over the whole range of points is  $a_w = 1.0001186 - 0.50250 \times (\text{mass fraction})^{2.79}$ . The exponent was found from the slope of the regression line (excluding the  $a_w = 1.0$  point) in the log–log plot, a value of  $2.79 \pm 0.08$ , which is the value  $\pm$  the standard deviation.

### 3.4. Characterizing the origins of the break in concentration dependence

#### 3.4.1. The uncertainties of PEG densities in solution

Before continuing, we briefly address the problem of attributing an exact proportion of solution volume changes separately to the solute or the solvent. For the PEGs, at 25 °C the density of the neat liquids ( $M_W$  200 to 600) is  $1.13 \text{ g cm}^{-3}$ , and the solid PEGs ( $M_W$  1500 to 6000) have a common density of  $1.21 \text{ g cm}^{-3}$  [25]. (This density equals, within its precision, the numerical value that is given in the reference, which is the specific gravity at 25 °C compared to water at 25 °C—denoted  $d_{25}^{25}$ ) The higher density of  $1.21 \text{ g cm}^{-3}$  is characteristic of crystalline PEG since, as Pielichowski has measured from his samples [26], neat, solid PEGs in the same molecular weight range that we used are greater than 85% crystalline. However, Sandell & Goring [14] found by dilatometry that the partial density of PEG 1000 spans a range from 1.13 to 1.21 between 25 °C and 5 °C and PEG 200 from 1.12 to 1.19 over the same range.

If the neat material's density appears to be less than its partial density in solution, is the water dilated or the average volume of the molecule increased or some of both? And if the density of the neat material is greater than the partial solution density, is the molecular volume compressed or the water density increased? Further, if the PEGs in solution are tightly packed like the solids, then with the apparent density in solution being the same 1.20, the *net* effect on the water is no perturbation, but we have no way to determine what combination of volume changes leaves the apparent density constant. This ambiguity makes separating the spectroscopic properties into those of the PEGs and those of the solvent uncertain, especially with higher concentration PEG solutions.

A further example of the enigma of PEG solutions is to compare quantitative compressibilities. Neat PEG 2000, a waxy solid, exhibits an isothermal compressibility that is typical for many organic substances [27]:  $0.39 \text{ GPa}^{-1}$ . Water's compressibility is in that same range [28]: at 20 °C,  $\kappa_T$  is  $0.46 \text{ GPa}^{-1}$ . A composite [29,30] compressibility [3] relative to pure water is proportional to the volume fractions of each times its individual compressibility. At 15% weight fraction PEG, with PEG's density 1.20, the PEG volume

fraction is 0.128. The value expected is, then,  $(0.872 \times 0.46 + 0.128 \times 0.36)/0.46 = 0.97$ . When compared to the conventionally measured compressibility value of 0.88 as shown in Fig. 5, we find that the mutual modifications of the water and PEG structures results in a solution bulk compressibility significantly smaller than a simple linear dependence in the mixture. This suggests a significant change in solvent and/or PEG structures when the two are mixed, and they form a significantly less compressible combination. This is reflected in the compressibility as measured by SANS. This significant change in compressibility cannot, as noted above, be attributed separately to the PEG or the water, nor can a reasonable partitioning of some fraction to each component be made. However, the change in the infrared absorbance can be separately attributed, as shown below.

### 3.4.2. Compare the Raman and IR concentration dependencies

Under these experimental conditions of salt, pH, and PEG molecular mass, above about 20% mass fraction, the 2000, 4000, and 8000 PEGs are seen to be gels with their SANS scattering—the same for all molecular weights. As a result, the upper concentration investigated was below that level. Infrared and Raman spectra were obtained from a set of solutions of the six different molecular masses (200, 400, 1000, 2000, 4000, 8000) each at a set of six different concentrations (percent mass fraction): 1, 3, 5, 9, 13, 17% for the infrared and 2, 4, 6, 10, 15, 20% for the Raman.

The band shapes of the PEG vibrations do not vary with concentration within experimental uncertainty. As a result, only the peaks were used to characterize the changes. We were unable to use modeled underlying individual component bands for analysis, because small uncertainties in the baseline produced

significantly different optimum sets of component fits. Also, even with a chosen, fixed baseline, these fits were seldom unique. Without further data to establish the correct numbers of bands and to determine the baselines and whether they change with the PEG concentrations, the data analysis will have to depend on vibrational peak heights.

With that limitation, we see only a few band peaks change systematically with molecular weight with the concentration fixed. See, for example, Table 1 for 13% solutions. (Other values can be seen in the tables of the Supplement.) As was seen from the IR spectra of Fig. 3, especially below  $1000 \text{ cm}^{-1}$ , the secondary structure (that is, the form of folding) of the PEGs of 2k, 4k, and 8k differ from those of 400 Da and 600 Da. The 1000 Da PEG lies on the border between them.

On the other hand, with changes in the concentrations, the positions of the PEG peaks show no clear, systematic changes. Also, as noted previously for Fig. 6, the peak intensities show a break in trend with concentration. However, as shown in Fig. 8, over this same range of concentrations, the Raman spectra show no break in the trend of intensities, only the expected linear proportional increase in scattering with concentration for each band.

Both for the water and for the PEG, the positions of the vibrational bands are highly sensitive to structural changes [31]. However neither the infrared nor Raman peaks of the PEGs shift with concentration, and, as noted immediately above, the intensities of the Raman peak heights are linear with concentration. Given the sensitivity of vibrational bands to structure, we must conclude that the break in the trends with concentration seen in all the measures described above does not arise from a significant change in the PEG structure. It follows that changes in the water structure

**Table 1**  
PEG IR band assignments and wavenumbers at 13% concentrations.

200 13% $\text{cm}^{-1}$	400 13% $\text{cm}^{-1}$	1000 13% $\text{cm}^{-1}$	2000 13% $\text{cm}^{-1}$	4000 13% $\text{cm}^{-1}$	8000 13% $\text{cm}^{-1}$	Oligo helix vanderah <sup>a</sup>	Melt <sup>c,g</sup>	Dissanayake amorphous	Crystalline <sup>b,e,f</sup>	Assignment <sup>a–g</sup>
2925	2923	2922	2922	2922	2922					$\nu_{\text{as}}(\text{CH}_2)$
2885	2884	2884	2884	2884	2884	2893/2816				$\nu_{\text{s}}(\text{CH}_2)$
		1712								Impurity in batch $\text{s}(\text{CH}_2)^{\text{f}}$
1470	1474	1474	1474	1474	1474					$\delta(\text{CH}_2)^{\text{f}}$
1459	1458	1458	1457	1457	1457		1460		1461/1454	Impurity in batch
			1396							w ( $\text{CH}_2$ )
1352	1350	1350	1350	1350	1350	1348	1352	1350	1358	w ( $\text{CH}_2$ )
1334	1333	1333	1334	1333	1333		1326	1325	1342	w ( $\text{CH}_2$ )
1299	1306	1302	1302				1296	1294		t ( $\text{CH}_2$ )
	1287	1286	1285	1286	1288		1285 R		1278	$t_{\text{as}}(\text{CH}_2) + t_{\text{s}}(\text{CH}_2)$
						1243		1250	1240	t ( $\text{CH}_2$ )
							1249		1236/1244	$t_{\text{as}}(\text{CH}_2) - t_{\text{s}}(\text{CH}_2)$
1134	1136	1136	1137	1136	1134	1149/1126	1140/1135	1142	1147	v C–O + v C–C
						1118		1110	1111/1116	Ordered 7 <sub>2</sub> helices, vCC
1096	1087	1084	1083	1083	1082				1092	Not assigned
1069									1060	$\nu_{\text{as}}(\text{COC}) + r_{\text{s}}(\text{CH}_2)$
1032	1035	1037	1037	1036	1038		1038	1040		v CO + more
990	990	992	993	991	989		992	993		v CO, vCC
						965			963	r ( $\text{CH}_2$ )
946	948	948	949	948	949		945	948	949	$r_{\text{s}}(\text{CH}_2) - \nu_{\text{as}}(\text{COC})$
918	915						915			r $\text{CH}_2$ + v CO
883	883	883	884				885 R			v CO + r $\text{CH}_2$
832	836	840	841	841	841		842 R		844	$r_{\text{as}}(\text{CH}_2)$
817	812		817				810			r $\text{CH}_2$ + t $\text{CH}_2$

Abbreviations:  $\nu$  stretching;  $\delta$  bending; t twisting; w wagging; r rocking; s scissor; R Raman.

<sup>a</sup> Lappi, Ref. [45].

<sup>b</sup> Dissanayake, Ref. [80].

<sup>c</sup> Matsuura & Fukuhara, Ref [81].

<sup>d</sup> Wang, Ref. [82] (2800–2900 region).

<sup>e</sup> Yoshihara, Tadokoro, Murahashi, Ref. [83].

<sup>f</sup> Miyazawa, Fukushima, Ideguchi, Ref. [84].

<sup>g</sup> Koenig, Angood, Ref. [85].

<sup>h</sup> Not included are terminal methoxy bands at  $2979 \text{ cm}^{-1}$  and  $2917 \text{ cm}^{-1}$ .

<sup>i</sup> HOD bend lies underneath these.

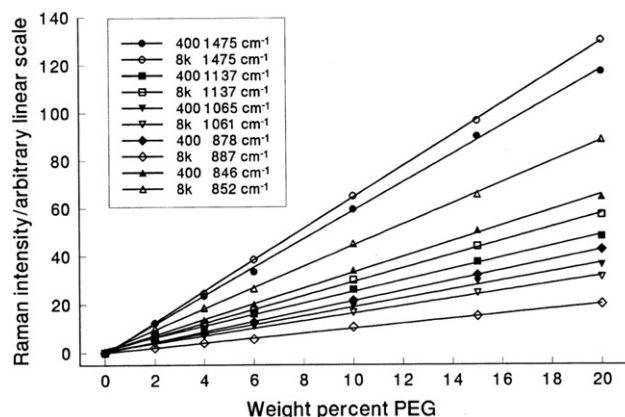


Fig. 8. Raman peak scattering versus weight percent PEG for selected bands for PEG 400 and PEG 8000 in  $D_2O$  that, unlike the infrared spectra, show no discontinuities.

causes the break. The interpretation of an unchanging PEG structure coincides with an understanding that the structure can be averaged over the relaxation times of the infrared vibrations. This limitation does allow averaging over structural changes due to proton transfers, which in the realm of water structure permits pseudorotations and small pseudotranslations of the waters within this averaging time frame.

### 3.4.3. The nature and cause of the absorption coefficient change

The PEG unique properties of having an unchanging wavelength and an absorption coefficient with two different values depending on concentration can only be explained in general terms. However, the uniqueness of the properties can eliminate many possible causes as seen experimentally or explained in theory. For example, the classical reaction field cannot change enough and leave the frequencies fixed over the concentration range [32]. In addition, the changes in the intensities with dielectric properties are generally less than 10% [33] and usually peak positions shift significantly as well [34]. The dielectric constant of water over the IR region ranges from 1.1 to 1.5 [35]. This suggests that we should expect absorbance changes of less than 10% from this cause as seen from the prior work cited.

Infrared absorbance changes of the magnitude we see here were reported by a number of groups [36–38]. However, these significant changes in absorbance found over temperature scans were accompanied by significant changes in frequencies that were attributable to conformational changes that mixed various modes. As a result, these earlier absorbance changes are not considered to be comparable to the PEGs.

To explain the lack of any significant shift in band wavelengths given the sensitivity to structural changes of vibrational spectroscopy, the PEGs' average structure must not change with concentration. Similarly, if water is bound tightly to the PEG, then the average structure of the two together does not change. As a result, we must conclude that the change in absorption arises from the influence of many layers of water that shift in structure and cause the absorbance changes. It follows that this soft structural change results in a significantly different relaxation rate for energy to flow from the PEG to the solvent and in doing so results in different PEG and water absorption coefficients [39].

We cannot tell whether the change in relaxation rate arises from a change in the density of states of the solvent allowing a more efficient vibrational solute-solvent energy path or whether the mechanism might be more concerted such as some deuterium exchange that occurs faster than the infrared relaxation rate [40].

We do know, however, that the O–H/O–D vibrational bands do extend over a number of adjacent waters [41], which is especially clear from the frequency dependence of water bands depending on the H/D ratio of the solvent [42–45]. As a result, the dependence on more than the first hydration layer is not unexpected. Further, numerous studies have shown that pure water consists of two different states [46–48] with a relaxation rate change that depends on the net number of hydrogen bonds [31]. We do not need to consider the intramolecular vibrational relaxation since it is fast relative to the solute-solvent rates [49,50].

The nature of the shift in solvent structure is not approachable in detail with the data at hand. However, we can say that the PEGs and their most tightly bound waters must be “hard” in order to retain their structures while the solvent structural change that results in the different absorption coefficients should be characterized as “soft.”

Two different trends provide further information about the mechanism for the change in absorption coefficient. First, the ratios in slope on either side of the absorbance transition for all the molecular masses tends to increase as the infrared frequency decreases. (Tables are provided in the *Supplementary Materials*.) In other words, from a general perturbation viewpoint, lower frequency modes of the solvent are more effective in changing the rate of relaxation. The second trend is that the differences in the slopes tend to increase with molecular mass. From the discussion above, this suggests that the narrower the range of PEG structures allowed (or simply the length of the molecule), the more effective is the solvent structural change to modify the relaxation rate. This trend may depend on the PEG flexibility or on the structural order of the water or both; we suggest that pump-probe experiments on the same solutions would be enlightening in unraveling the mechanism.

In this discussion, we should note that the PEG 8000 differs from the lower molecular mass PEGs in that not only is the slope ratio significantly larger, but the line segment fitting the higher concentration set jumps up so that the higher concentration and lower concentration lines do not intersect between the 5% and 9% points as do the others. With only one molecular mass showing this behavior, we can only suggest that the jump is due to a simultaneous absorbance change in the underlying, broad background. That possibility further suggests that at least some of the PEG 8000 concentrations have a hydration structure that itself differs in some significant manner. For the time being, we classify the PEG 8000 behavior as an outlier and omit its specific characteristics in the discussion of changes in the spectrum.

### 3.4.4. Changes in the water: the infrared spectrum and stoichiometry

The areas of the water O–D vibrational region were obtained between the two isosbestic points at  $2775.5\text{ cm}^{-1}$  and  $2000.0\text{ cm}^{-1}$  for all the molecular masses and concentrations. These values are plotted in Fig. 9 where the similarities in behavior for all but the PEG 8000 can be seen. Although the points are plotted for PEG 8000, we ignore them in this discussion.

The extrapolations of the areas to zero PEG concentrations are shown in Table 2, and they agree within a few parts per thousand. These are the zero extrapolations of the lower straight line of Fig. 9 following the lower concentrations. The linear extrapolation of the higher concentration points lies uniformly about 2% higher than those in the lower concentration range.

The slopes versus concentration of the integral areas on each side of the break along with the ratios of the slopes are listed in Table 3. We have ignored the effects of deuterium exchange with the terminal hydroxy hydrogens since even the maximum contribution—that by the 17% solution of PEG 200—causes less than

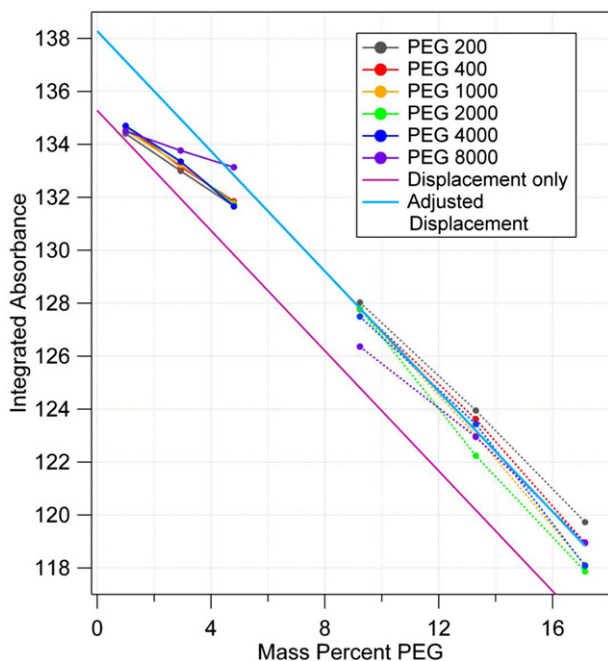


**Fig. 9.** Area in (absorbance units wavenumber) of the main vibrational D<sub>2</sub>O band as it changes with PEG concentration together with the trends expected from displacement alone. The lines extend from the two zero points found by extrapolation from the concentration ranges both below and above the break in the absorbance trend.

a 2% change in the O–D content of the solvent (i.e., less than 2 M of 110 M).

Let us now compare the measured absorbances to those expected simply from displacement of the water by the solute PEGs. In Fig. 9, the lower straight line projects from the average of the zero-solute value (135.28 assuming the PEGs have a common partial density of 1.2 and the light-water density is 0.99777 at 22 °C). The higher line falls from the projected intercept (138.3) found from the three highest concentrations for each molecular weight. As can be seen, the higher line captures the trend of the higher concentration data although not some details. The upper sloping line shows that the water absorbance follows from water displacement alone but with an absorbance about 2% higher overall than found from the zero projections of the lower-concentration sets of points.

It is clear from the graph that the change in water absorbance is occurring linearly with PEG concentrations up to the 6% concentration range where the final, higher absorbance is reached. The intersection with the higher trend line coincides with a molar ratio of water to EO monomer of about 32.

We now treat the IR versus concentration data as a titration of water by PEG detected by IR. First, compare the average low-concentration slope (of PEGs 1000, 2000, 4000) and the slope expected from displacement alone. This ratio is 1.6 (inverse 0.62). Then compare the ratio of the extrapolated zero PEG “pure water”

**Table 2**  
Regression to zero PEG concentration of integral areas 2775.5 cm<sup>-1</sup> to 2000.0 cm<sup>-1</sup> (O–D stretching region).

PEG molecular weight	Intercept low-conc region (val ± s.d)	Intercept high-conc region (val ± s.d)	Relative change high/low (val ± s.d)
200	135.12 ± 0.02	137.8 ± 0.4	0.020 ± 0.003
400	135.40 ± 0.08	138.2 ± 0.8	0.020 ± 0.007
1000	135.29 ± 0.08	139.1 ± 0.4	0.028 ± 0.004
2000	135.5 ± 0.2	139.2 ± 0.9	0.027 ± 0.008
4000	135.6 ± 0.2	138.7 ± 1.6	0.02 ± 0.01
8000	134.8 ± 0.1	135.1 ± 0.8	0.002 ± 0.007

**Table 3**  
Slopes of graphs of area O–D stretch versus mass percent PEG in solution.

PEG molecular weight	Slope ± s.d. low (% conc) <sup>-1</sup> PEG	Slope ± s.d. high (% conc) <sup>-1</sup> PEG	Ratio slopes H/L
200	-0.721 ± 0.006	-1.05 ± 0.03	1.46 ± 0.03
400	-0.75 ± 0.02	-1.11 ± 0.06	1.48 ± 0.06
1000	-0.73 ± 0.02	-1.22 ± 0.03	1.67 ± 0.04
2000	-0.77 ± 0.05	-1.26 ± 0.06	1.63 ± 0.08
4000	-0.80 ± 0.06	-1.2 ± 0.1	1.5 ± 0.1
8000	-0.36 ± 0.01	-0.9 ± 0.6	2.5 ± 0.6

intercepts from the two concentration ranges: this value is 1.026. In other words, the PEG changes the absorbance of the solvent it influences by 60%, which results in an overall change of 2.6% in the absorbance of the total solvent. The end point of the titration is reached at about 32 waters per EO after which no further changes in absorbance are generated beyond simple displacement by more PEG.

Of the 32 waters associated with each EO of the PEGs, we do not know what fraction has its absorbance changed; it could be 32 with 2.6% change or some minimum number changed by 60% or any set of the numbers in between with the same mathematical product. However to have the minimum number of waters affected by the changing PEG concentration, only the fraction  $2.6/60 = 0.043$  of the 32 waters is affected. That is,  $32 \times 0.043 = 1.4$  waters per EO have a 60% change in absorption coefficient. As a small whole-number molar ratio, there are three waters affected for every two EO groups.

### 3.5. Water energetics and length scale

The discussion in this section is based on the point of view of a titration of water by PEG carried out with vapor pressure osmometry detection. The discussion uses: 1) the values of the water activity  $a_w$ , which is the data plotted in Fig. 7; 2) the stoichiometry of the PEG–water solutions at the property-trend break; and 3) the assumption that this break results from a structural change of the solution.

As was described above and plotted in Fig. 7, the addition of PEG initially leads to only minuscule changes in the solution's water activity. This means that at least some of the water remains close to its original state in the solution. In other words, if the PEGs are isolated in some manner from the water, the water activity will be essentially unaffected. This near elimination of the effect on the water activity of the presence of the PEGs follows from deep hydration, i.e., having a number of layers of water over the solute surface with each one shielding those closer to the surface so that the outermost layer remains nearly energetically equivalent to pure water. The solvent molecules in the outermost layer then become the representative of the bulk property. How this behavior compares to the standard colligative properties of water are addressed more below.

The effect of layer shielding can be seen through the interesting relationship shown in Fig. 7b: this one for PEG 6000 at 20 °C. The slope of the regression line for the measured  $\log a_w = \Delta G^\circ$  versus log of the weight percent PEG is 2.8 over the entire measured range. The free energies of the waters becomes more negative with increasing PEG:water ratio, and the decrease is linear with the ratio's logarithm over the whole region—where the H<sub>2</sub>O:EO ratio varies from 22 to 6. In the following section, we will use information from the SANS experiments to connect that concentration-ratio dependence to a distance dependence. First, however, we briefly derive how interpreting such data requires recognizing the characteristics of the free energy per unit volume.

For the water evaporating from the solution surface, we recognize that the free energy calculated from the isopiestic water-activity measurements applies to each individual, escaping water

molecule. Without knowing the details of the water/vapor interface for the PEG solutions at the atomic length scale, we assume that the water molecules escaping from the surface have, on average, the same free energy as those exchanging at the outer hydration layer—that is, the region furthest removed from the PEGs' surfaces. At the break point of the infrared absorbance and the other properties—say 8% PEG as the highest concentration—the interpolated water activity coefficient is 0.9996. From this, we calculate at 20 °C that  $\Delta G^\circ = -RT \ln a_w = -582 \times 2.303 \log 0.9996 = -0.24 \text{ cal mol}^{-1}$ —only a quarter of a small calorie. On the other hand, to have an observable structural transition requires approximately  $k_B T = (RT/N_A)$  of energy change, which is  $2.4 \times 10^3$  times as much as the individual water molecules as measured from the experiment.

We ask, then, If all the waters involved in the structural transition have the same free energy, what is the volume of the water that can exhibit such a structural transition? For a mole of water occupying 18 mL, the fractional volume for each water is  $30 \text{ \AA}^3$ , and  $2.4 \times 10^3$  waters will fill a cube approximately  $42 \text{ \AA}$  on a side. From this simple calculation, we must conclude that these thermochemical measurements made on the PEG solutions involve two different length scales. The smaller one, that of the water's activity measurement is about  $3 \text{ \AA}$ , and the larger one, that of the solution structure change, is at least  $40 \text{ \AA}$ ; these lengths differ by more than an order of magnitude. Even though the  $\Delta G^\circ$  becomes more negative spatially closer to the PEG molecules, which makes this simple calculation incorrect in detail, its value still remains the correct order of magnitude.

As is well accepted, the vapor pressure of a solution is a colligative property, which, for the ideal case, is generally understood to result from the increase in entropy in the solution compared to the pure solvent. It occurs due to the entropy of mixing, which reduces the chemical potential [51]. However, an underlying assumption is that the molecular volumes of the solvent and solute are the same, which is not the case for polymer solutions. Many adjustments have been suggested to compensate for such solute-solvent size mismatches [52–55]. Here, the preference is to view the changes as due to the different length scales of the measurements: that of  $a_w$  and that of the change in the solution structure leading to the change in, e.g., the IR absorbance.

The general necessity of asking on what length scale a thermochemical effect occurs was addressed by Rowlinson [56] who, among others [57,58], associate an energy density or free energy density with volumes within a solution. Rowlinson noted that the limits of thermodynamics are those of the correlation length in the materials being measured, a quantity that is much more commonly associated with scattering experiments. The correlation length is a length characterizing the inhomogeneities in the solution; below that length, there is no significant thermodynamic difference for the chemical structures involved. An alternative way we can state this idea here is that no static structural inhomogeneities show up over such distances unless the free energy is on the order of  $k_B T$  or greater over that distance. At energies lower than  $k_B T$  over a distance, one is, in essence, in the bulk at that length scale. The bulk may be either in the solvent region or in the polymeric solute region. Another alternative statement of this characteristic is that, among other structures, interfaces extend on the order of the solution correlation length. In a simple liquid, the correlation length is about  $10 \text{ \AA}$ , and the volume associated with that approximates  $L^3 = 1000 \text{ \AA}^3$ . For the PEG solutions, the correlation length appears to be significantly longer—about the longest dimension of the polymer.

The existence of a structure that only shows up over distances many times those of the solvent molecule size in the liquids has been found in other measurements. For example, in water Jansson [59] measured a slow dielectric relaxation of a Debye character with a peak at 4 MHz—five orders of magnitude slower

than the  $\alpha$  process below 37 °C (The Debye character is defined by an exponential relaxation and modeled as arising from a noninteracting population of dipoles [20,60]) In water, among other hydrogen bonding liquids, a Debye relaxation is believed to arise from the collective motion of hydrogen-bonded structures, and the distance associated with this collective motion is estimated to arise from interactions over a distance of about  $10 \text{ \AA}$  [59].

The mechanical properties of the liquids further support the presence of longer correlation lengths in the form of collective interactions over longer distances in “nonequilibrium states in large groups of molecules”. [61] Derjaguin et al. [61] showed that with a low frequency mechanical perturbation, a number of liquids including water exhibit solid-like shear elasticity. In addition, Noirez et al. [62] demonstrated that the mechanical relaxation of liquid glycerol when done with small displacements and without slip at the perturbing surface behaves as an elastic solid [63]. At higher displacements, the elasticity vanishes, and conventional liquid behavior returns.

In the PEG solutions, the distances/volumes necessary to collect  $k_B T$  energy from the water are at least as large as the PEG molecules themselves. From neutron scattering data we can discover the structure of the PEGs in the solvent, and that is the topic of the next sections.

### 3.6. The intramolecular and intermolecular structures of PEGs in water

#### 3.6.1. The intramolecular structures

Prior work [4] with neutron scattering obtained on PEG solutions similar to those here has concluded from the radii of gyration of the molecules in dilute solution—as listed in the first column of Table 4—that the PEGs are, indeed, solitary polymer molecules in dilute solution. But those values do not provide information on their shapes.

The possible shapes are limited by the trend in the radius of gyration  $R_g$  with molecular weight. The mass dependence requires a structure either of a plate or of a random coil [4]. This dependence eliminates from consideration ellipsoidal aggregates such as proposed by Thiagarajan et al. [7] The elimination of the random coil model rests simply on the presence of broad peaks in the SANS curves at the higher concentrations for the PEG 2000, 4000, and 8000. Only individual scatterers can produce a peaked scattering curve. Polymer random coils overlap and do not exhibit peaks in such scattering curves. (Log–log graphs of  $I(q)$  versus  $q$  for these are shown in the Supplement.)

Another model, scattering from a solution of solvent-expanded polymers, can be fit to some of those scattering curves. However, this model is incompatible with other data: 1) the presence of the broad peaks at higher concentration, and 2) apparent  $R_g$  values of that model that change significantly with concentration. The possibility of the apparent change is contradicted by the unchanging infrared band frequencies. The model of PEGs as solvent-expanded polymers under these conditions is invalid.

In addition, from neutron scattering results not illustrated here, gels do not form until the solutions are approximately 20 mass percent, which also indicates a lack of overlap at these lower concentrations.

The only valid interpretation remaining is that the scattering arises from PEGs that are flexible plates one molecule thick for the molecular mass range from 2000 Da to 8000 Da. The dimensions of these plates are listed in the first column of Table 4 [4].

By eliminating Gaussian chain or expanded Gaussian chain structures, we are forced to accept that the structures of these PEG molecules are flat. It is worth noting that NMR experiments measuring rotational diffusion for a range of PEGs in the same

**Table 4**  
Intermolecular model results for  $S(q)$  curves.

Sample (~molecular dimensions) $R_g/\text{\AA}$ from fits <sup>a</sup>	PEG concentration% w/w	Av intermolecular dist/ $\text{\AA}$ from peak $S(q)$ ( $\pm$ est read error)	Model plate Separation <sup>b</sup> ( $\text{\AA}$ )	Separation/Av number waters @ 2.5 $\text{\AA}$ separating sheets = $2 \times$ depth of hydration (s.d. in last digit)	Calculated intermolecular N1 neighbor distance/ $\text{\AA}$ <sup>c</sup>
PEG 2k ( $20 \times 42 \times 4$ ) 16	3	50 (4)	22	8.8 (3)	111
	5	35 (2)	15	6.0 (3)	93
	9	26 (2)	11	4.4 (3)	77
	13	22 (2)	10	4.0 (4)	68
PEG 4k ( $28 \times 78 \times 4$ ) 24	3	48 (6)	22	8.8 (3)	140
	5	35 (3)	14	5.6 (4)	117
	9	27 (3)	12	4.8 (4)	96
PEG 8k ( $42 \times 100 \times 4$ ) 31	3	41 (4)	18	7.2 (3)	176
	5	32 (3)	15	6.0 (3)	148

<sup>a</sup> From Ref. [4], 0.5% solution.

<sup>b</sup> Estimated reading uncertainty in peak matching:  $\pm 1 \text{\AA}$

<sup>c</sup> Assumes the density of PEG in solution =  $1.20 \text{ g cm}^{-3}$  and N1 neighbors at the center of faces of a rhombic dodecahedron.

molecular mass range as used here indicated that the molecules were highly anisotropic [64]. In addition, light scattering and other methods evidence shows that PEG 400 [65] and smaller and larger oligomers [66] reversibly forms clusters, which indicates that we should expect the intrachain association of the higher molecular weight PEGs and not expanded, hydrated molecules forming under these conditions.

### 3.6.2. The intermolecular distances

The following discussion is based on the SANS intermolecular scattering curves found by calculating  $S(q)$  with Equation (2). The set of  $S(q)$  curves for PEG 2000 is shown in Fig. 10. In effect, without modeling any structure, the calculation produces from  $S(q) = I(q)/P(q)$ , where  $P(q)$  is the scattering from isolated molecules (assumed noninteracting in 1% solution).

A peak in the  $S(q)$  curves indicates the average intermolecular distance between PEG molecules as if they were uniform spheres. Modeling is required to find the distance between two highly anisotropic entities such as the slablike PEGs. However, to compare with the peaks in the  $S(q)$  curves, let us first calculate the expected center-to-center distances for each PEG concentration and molecular weight. That is, we calculate the expected distance between equally spaced scatterers in solution. To do so requires that each (central) particle be equidistant to its nearest neighbors (N1), and, just as importantly, the nearest neighbors are spaced from their nearest neighbors at the same distance. A calculation to find this distance as a function of concentration is straightforward since these stringent requirements are satisfied if twelve nearest neighbors reside at the centers of the rhombic faces of a rhombic dodecahedron. This shape is space filling through translation, and, as a result, models a solution of particles equally spaced with their nearest neighbors.

To carry out the numerical calculation, we note that the volume of a rhombic dodecahedron equals  $3.079 \times (\text{edge length})^3$  and contains seven particles in its volume—that is,  $12 \times \frac{1}{2} + 1$ . As a result, the number density of rhombic dodecahedra equals one-seventh the number density of particles. From that value, the volume of each follows. Then, from the geometry, the rhombic dodecahedron edge length and then expected particle separation can be calculated. The center-to-center value is

$$\begin{aligned} &\text{center - to - center distance (in \AA)} \\ &= 1.27 \times 103(\text{concentration in } \mu\text{M})^{-1/3} \end{aligned}$$

In Table 4, these distances are listed in the rightmost column. As can be seen by comparing these to the distance equivalent to the

peak in  $S(q)$  in column 3, the experimental distances are consistently less, which indicates association in some way of the PEG molecules in the solution. The similarities of the peak value distances with weight fraction for the three different molecular

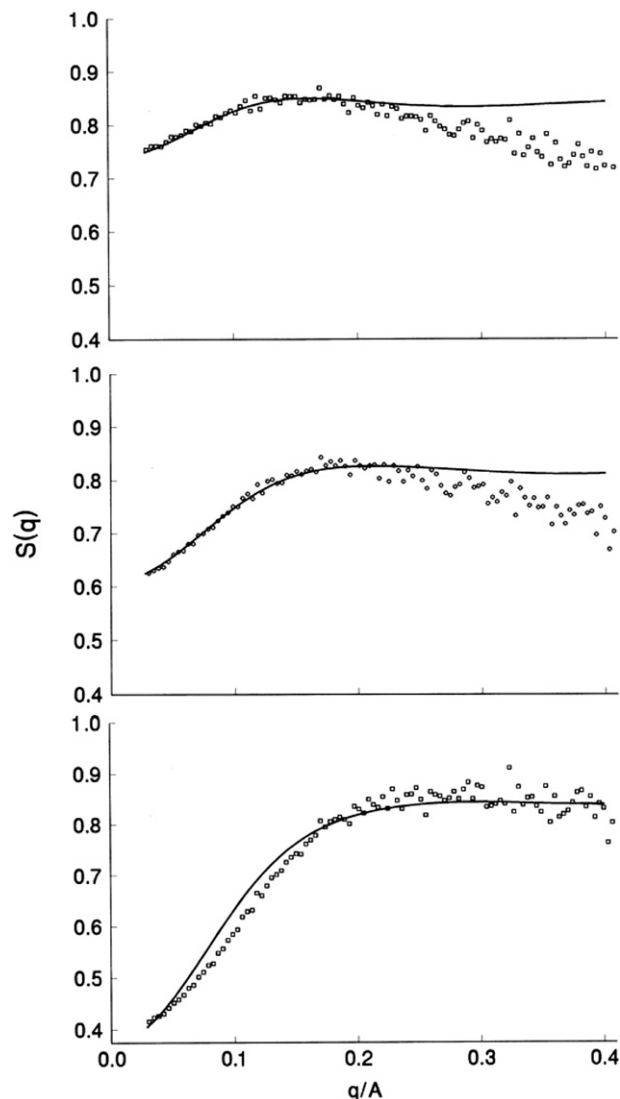


**Fig. 10.**  $S(q)$  and fits as rigid, paired sheets for PEG 2000 3%, 5%, and 9% solutions.

weights indicates that the controlling variable is the PEG-monomer:water concentration ratio.

Since the data indicates association of molecules that have sheet like structures, a more quantitative evaluation of the structures involved was undertaken. However, in order not to overinterpret the data and to make a simulation tractable, a significantly simplified model was developed. The structures were assumed to be rigid, flat plates the size of the PEG as given in the first column of Table 4. We expect that if any attraction occurs between them, then they will align with the large dimensions parallel and face-to-face. In addition, they should have their edges aligned since the attraction will be maximized if they completely overlap; any offset would reduce the area of attractive interaction. As will be discussed below, we expect that the plates are not rigid, and the differences between the calculated scattering of the rigid intermolecular structures and the experimental curves support that interpretation. In addition, pairs of plates were satisfactory in explaining the data, and a stacked triplet was not better. In effect, we cannot eliminate stacks of many layers, but if such stacks exist, the correlations between them die out beyond the nearest neighbor.

By using this simplified model, we only attempt to match the  $q$  at the peak, but the calculated curve is scaled to fit as much of the experimental data as possible. Fits for the PEG 2000 solutions of 3%, 5%, and 9% are shown in Fig. 10. The plate separations, found from the model when the model's peak matched the  $S(q)$  data peak, are listed in the fourth column of the table. The number of layers of water molecules that will fit into that spacing appears in the fifth column. The thickness of a layer is taken to be 2.5 Å as found from AFM measurements of water on mica [67], which is described in greater detail below.

The two regions on either side of the peaks show some discrepancies between the model fits and the data. Both provide useful information about the structures. First, the departure on the high- $q$  side of the data (to the right side), where the data points lie below that of the rigid model, can occur when the correlation is not as high as modeled by rigid structures. This lower correlation can occur when the molecules have a distribution of structures—when it is flexible. As noted earlier, evidence of such flexibility appears in the infrared spectra, where the shorter PEGs appear to be have more conformations. We expect that the ends of the chains are disordered in the same manner. Further, we see that the data departs from the rigid model at  $q = 0.25$ , a distance of about  $6.28/0.25 = 25$  Å for the lower concentrations. This is the width of the plates for PEG 2000 with the implication that the pairing is structurally flexible.

Significant flexibility on short length scales is also apparent. Bieze et al. [68] obtained higher-angle neutron scattering in the range  $0.6 \text{ \AA}^{-1} < q < 13 \text{ \AA}^{-1}$  to probe the local structure of PEGs in this mass range. No structured water was seen, and the intramolecular correlations extended only to  $\approx 5$  Å. The measurement used PEG 14,000 and *d*-PEG 11,200.

On the low- $q$  side of the peak, the 3% and 5% solutions fit quite well, and this is not surprising since below  $q \approx 0.14$ —equivalent to the longest length of the molecule—the scattering arises from the entire molecular mass, and this curve shape is characteristic of SANS scattering. The discrepancy for the 9% solution may arise from a few different structural effects: 1) Crowding in the solution means that the model of solitary individual pairs is no longer a good approximation. 2) The separation of intramolecular and intermolecular components— $S(q)$  and  $P(q)$  respectively—does not hold over the entire range since the molecular shape does not remain the same.

### 3.7. Pairing and the deep hydration of PEGs and other examples

Let us now turn to the structure of the PEG pairs separated by water and the cause for their formation. Their structure can be

understood simply as two hydrated plates that have layers of waters that decrease in binding energy as the distance from the plate surface increases. By quantitating the separation of the plates as it changes with PEG concentration, we postulate a method to assign free energies to individual layers by connecting the local, molecular level information with the bulk measurement of  $d_w$ .

The pairs themselves form because the PEGs are binding waters sufficiently deeply that they bind *across* the midpoint of the separation of the plates. In other words, the water mediates the pairwise attraction; it is strongly bound enough at the middle to hold the molecules together. On the other hand, in order to bring the molecules closer together, an entire layer of water must be removed (with the approximation of sufficiently stiff plates). For PEG 2000, approximately 140 waters must be removed, and proportionally more for the higher molecular weights. In other words, the total energy required to remove the layer means that the mediating water also holds the plates apart. The attraction and repulsion are two sides of the same water mediation; they are not independent. A similar viewpoint was put forth by Leikin et al. [69] but with data from a much more concentrated solution of collagen. Quantitation of the energies here will provide more insight.

While the free energy change is attributed to water alone, our system contains 10 mM of phosphate buffer near neutral pD and 10 mM KCl. By holding the pD near neutral, the possibility of deuteron binding has been minimized while simultaneously minimizing potential hydrolysis. The binding constant of  $K^+$  is expected to be low given the data cited in the Section 2.1. As a result, binding of  $K^+$  to PEG in 10 mM KCl buffer will be neglected as contributing to the pairing or perturbing the measured water activity outside of experimental uncertainty.

A number of other chemical structures explicitly show numerous layers of hydration. Water itself might be considered deeply hydrated since it has ordered structures that are observable by scattering; the O–O structural correlations are observed clearly up to 8 Å depth [70].

Another example, and perhaps the best known, is the fixed spacing between bilayers in multilayer liposomes [5,6]. In the presence of excess water, the spacing between the bilayers are in the same 20 Å to 30 Å range detected here at the low concentrations of PEGs, and the spacing does not depend on ionic strength [5].

Through the use of a number of complementary techniques, Filfil and Chalikian [71] inferred that upon binding of turkey ovomucoid third domain to  $\alpha$ -chymotrypsin,  $452 \pm 22$  water molecules were released to the bulk. However, over the contact surface area, the first hydration layer consists of 171 waters, which means that  $2\frac{1}{2}$  water layers are released.

An even deeper effect on the water layer is found from the depth of a smooth water layer adsorbed on quartz surfaces at equilibrium, and it is strongly dependent on the surface wetting characteristics. Depending on the surface, the equilibrium thickness of the layer can differ by more than 100 Å at 25 °C with the vapor pressure at 0.975 of saturation. [72].

Zheng et al. [73] using a number of different methods found that hydrophilic surfaces produce a zone for distances up to 100  $\mu\text{m}$  where the water is less mobile than the bulk. In addition, this less mobile region causes solutes such as proteins to be excluded from the volume.

However, even without the mass transfer required for mobility, the orientational correlation length of molecular liquids including  $D_2O$  appears to be greater than 5 nm. This conclusion was found by second-harmonic Rayleigh light scattering on the liquids [74]. A more precise correlation length for water requires more theoretical advances.

Similarly, on a mica surface in a solution of 10 mM KCl, Jeffery et al. [67] observed increases and decreases in damping (viscosity) and stiffness over a countable seven water layers as an AFM tip approached the surface.

Recently, Fameau et al. [75] found that some mixed hydroxyalkyl-amine-12-hydroxy stearic acid bilayers formed multilayer tubes with interlayer spacings. The interlayer spacings depend on the alkylamine chain length and on temperature and lie in the range of 200 Å to 400 Å.

On shorter distance scales,  $K^+$  ions show evidence of a second hydration shell with enough correlation to show up in neutron scattering. [76] And the aqueous solution structure surrounding *t*-butanol appears to have order up to the third hydration shell along the direction of the alcoholic hydroxy group [77]. Again this was found by neutron scattering. In addition, Heyden et al. [44] using pulsed THz spectrometry on aqueous solutions of carbohydrates found that the solutes effect the dynamics of hydration shells to a depth of  $\approx 6$  Å. The depth depends on the molar concentration of the solute and the number of hydrogen bonds with waters. That is, the larger carbohydrates had an effect deeper into the hydration layer. The same group [78] found that the changed dynamics of the hydration layer surrounding a protein extends at least to a distance of 10 Å, equal to four layers of hydration.

### 3.8. Assigning free energies to the hydration layers

To make the assignment of free energies to hydration layers requires that we relate the measured water-activity/free-energy over the concentration range to the changing distance between the paired PEGs. To relate a structure on the molecular distance scale to a macroscopic measurement requires a few assumptions. First, we assume that the hydration extends outside the PEGs half the distance between them. Second, we also assume that the free energies of the waters of the layers between the pairs of PEG molecules are the same as the corresponding layers on both outsides of the pairs of PEG molecules. As a consequence, to remove a layer between a pair of PEG molecules, we must remove that layer and the two approximately energetically equivalent ones outside the pair. Numerically, if 150 waters fit in a layer between a pair of PEG molecules, around 450 need to be removed to bring the pair of PEG molecules closer together by one layer thickness.

The distances between the plates at the various concentrations of PEGs are listed in column 4 of Table 4. Half this distance is assigned as hydration waters belonging to each side of the PEGs. From the average thickness of a layer, we can relate the thickness to the number of hydration layers. One choice for the layer distance may be the peak of the O–O correlation length from water scattering, which is  $(2.80 \pm 0.02)$  Å [70]. Another choice is the hydration layer spacing at a mica surface found by AFM as measured peaks and valleys as the surface is approached. The average peak-to-peak length found was  $(2.5 \pm 0.3)$  Å [67]. We choose to use the 2.5 Å length as applicable to the conditions found for the PEG hydration. With that divisor, the equivalent number of water layers is the

values shown in column 5. As stated before, half this number of layers is assigned to each side of the individual PEGs.

We can now ask about the stoichiometric information at the structure break at about 6% PEG. There, interpolation indicates that the plate separation of the PEG 2k and 4k to be 13 Å to 14 Å, with, then, about five layers of water between plates. This also means that about 2½ layers of water are attached to each side of the PEG. Since an ethylene oxide monomer in the chain fits three waters along its length, there are 15 waters per EO on the two sides. Since 6% PEG in the water has a monomer EO concentration of 1.36 M., with 15 waters on each EO, 20 M water of the 55.5 M is, then, considered bound.

We now must calibrate the local measurement of 20 M water bound with the measurement of  $a_w$  that follows from the macroscopic surface vapor pressure. Within the constraints of the approximations, we can relate the activity of the outer layer of water to the macroscopic measurements by finding the macroscopic water activity when the least strongly bound water that exists in the solution comes from that distance away from the PEG surface. In other words, we assume the local structure around the PEGs with their spacing in the solution remains the same when the bulk solution has the same stoichiometry. This assumption is not easily supported since the PEGs will approach closer together as the PEG:water ratio is increased to the more concentrated point. But such an approximation is necessary to connect the nm scale to the macroscopic thermochemical measurement. The calibration may be skewed by a layer of water, but similarly, the bulk escape capability of the waters at the surface are connected to the bulk properties with similar uncertainties at the nm scale for such solutions.

With these caveats, the outer layers of waters of the PEG 6% solution are then relatable to a solution with a weight percent PEG of 14.2% with a monomer EO:water ratio equal to 15, and the value of  $a_w = 0.99797$  by interpolating from Großmann's values for PEG 6000. With that activity at 25 °C,  $\Delta G^\circ_{\text{water}} = -1.18$  cal mol<sup>-1</sup>. We assign this value to the outer "half layer" of waters binding the PEG and also to the central layer of the five between the PEGs. In the same way, the free energy assigned to pairs with four, three, and two waters between them (outer layers 2, 1½, and 1) are found, and these are listed in Table 5.

These small free energies set the quantity of waters that are required to amass a  $\Delta G^\circ$  of  $k_B T$  compared to the standard state of pure, bulk water. The number of waters to "collect"  $k_B T$  for the four, three, and two separation layers  $\approx 1500$ , 750, and 300 to be removed from binding and transferred into the bulk water environment. Fewer waters are needed to equal  $k_B T$  closer to the PEG surfaces. As noted in the assumptions, we cannot differentiate between the layers outside of and between the PEGs.

.From the scattering results, all the PEGs form gels above about 20% PEG, which corresponds to an extrapolated 1.5 to 1.8 water interlayers. This is where  $a_w$  gives a binding energy  $\Delta G^\circ$  of  $-3.6$  cal mol<sup>-1</sup>. In other words, the gel forms as the second interplaner layer begins to be removed leaving only a single water between the polymer chains. The number of waters needed to

**Table 5**  
Layer free energies at 25 °C.

Interpolated number of layers	PEG 2000% concentration at which separation is $2 \times$ number of layers	PEG 4000% concentration at which separation is $2 \times$ number of layers	% concentration where overall stoichiometry equals separation hydration	Interpolated <sup>a</sup> $a_w$	Average $\Delta G^\circ$ of water layer in cal mol <sup>-1</sup>
4	2.8	2.9	9.5	0.99928	-0.4
3	4.0	3.7	12.2	0.99865	-0.8
2.2	6 (transition)	6 (transition)	15.7	0.99731	-1.6
2	8.1	9.1	17.4	0.99640	-2.1

<sup>a</sup> Data from Großmann, Ref. [1].

retain the structure in this intimate association between the water and PEG matches the conclusion reached by Assarsson [79] from vibrational spectra measured by neutron inelastic scattering as D<sub>2</sub>O was added to the solid: Namely that 8 to 9 waters per EO are needed to build a solvent structure capable of stabilizing the polymer. At that point the skeletal modes sharpened.

#### 4. Conclusions

Trends of measurements on aqueous PEG solutions indicate that the solution structure depends on both the molecular mass and PEG concentration. Vibrational spectra shows that the PEGs 1000 to 8000 are more restricted in structure than the PEG 200 and PEG 400 solutes. A change in solution structure is observed at approximately 6% mass fraction PEGs at constant pH and ionic strength. From the vibrational spectra, the change is attributable to changes in the water structure of multiple layers of hydration.

Neutron scattering data is consistent with PEGs that are separated by equilibrium distances that are less than expected from randomly distributed solutes in the solution. Consistent with the scattering data, the nominally 2000 Da, 4000 Da, and 8000 Da PEGs form flexible flat sheets, and a model of face-to-face sheet pairs can be used to relate the peaks of the intermolecular scattering to the intersheet distances as they vary with PEG concentration. As a representative value, a 3% solution of PEG 2000 has approximately 22 Å between the sheets, into which 9 layers of water 2.5 Å thick can fit. Through a calibration between the local structure at one concentration and the measurement of a bulk water activity at a different, related, higher PEG concentration, the value of  $\Delta C^\circ$  of  $-0.4 \text{ cal mol}^{-1}$  can be assigned to the fourth layer out from the PEG in the 3% solution.

It is noted that the thermodynamics of each measurement has an associated length scale. The length scale associated with the water activity measurement is in the range of 3 Å, and that for the water structural transformation around 6% PEG is in the range of over 40 Å. A similar dichotomy of length scales is expected to be needed to explain equilibria for solutions where a large number of waters change in concert on a length scale defined by a large solute. Protein–protein binding during crystallization is one class of such interactions. In effect, small free energies per unit volume of the outer layers of water molecules—on the order of  $-1 \text{ cal mol}^{-1}$ —are harnessed by the larger solutes to change in concert over a volume large enough to produce solution structural shifts differing in energy by greater than *RT*.

#### Acknowledgments

Small-angle neutron scattering experiments were performed on the NG3 and NG7 30 m SANS instruments at the NIST Center for Neutron Research. This equipment was partially supported by the National Science Foundation under agreement No. DMR-0454672. Also, thanks to Susan Krueger, Boualem Hammouda, and David Plusquellic for many useful discussions.

#### Appendix A. Supplementary data

Supplementary data related to this article can be found at <http://dx.doi.org/10.1016/j.polymer.2012.11.016>.

#### References

- [1] Grossmann C, Tintinger R, Zhu J, Maurer G. *Fluid Phase Equilibria* 1995;106:111–38.
- [2] Kalyanasundaram S, Sundaresan B, Hemalatha J. *J Polym Mater* 2000;17:91–6.
- [3] Rubinson KA, Hubbard J. *Polymer* 2009;50:2618–23.
- [4] Rubinson KA, Krueger S. *Polymer* 2009;50:4852–8.
- [5] Rand RP. *Ann Rev Biophys Bioeng* 1981;10:277–314.
- [6] Pabst G, Rappolt M, Amenitsch H, Laggner P. *Phys Rev E* 2000;62(3):4000–9.
- [7] Thiyagarajan P, Chaiko DJ, Hjelm RPJ. *Macromolecules* 1995;28:7730–6.
- [8] Bortel E, Makromol Kochanowski A. *Chem Rapid Commun* 1980;1:205–10.
- [9] Frensdorff HK. *J Am Chem Soc* 1971;93:600–6.
- [10] Ozutsumi K, Ishiguro S-I. *Bull Chem Soc Jpn* 1992;65:1173–5.
- [11] Yuldasheva LN, Hallwass F, da Cruz Gonçalves SM, Simas AM, Krasilnikov OV. *J Mol Liquids* 2003;106(1):31–41.
- [12] Lindoy LF. *The chemistry of macrocyclic ligand complexes*. Cambridge: Cambridge University Press; 1990.
- [13] Cabbiness DK, Margerum DW. *J Am Chem Soc* 1969;91:6540–1.
- [14] Sandell LS, Goring DAL. *J Polym Sci A-2* 1971;9:115–26.
- [15] Lepori L, Mollica V. *J Polym Sci Polym Phys* 1978;16:1123–34.
- [16] Cruz RDC, Martins RJ, Cardoso MJEDM, Barcia OE. *J Appl Polym Sci* 2004;91:2685–9.
- [17] Cruz RDC, Martins RJ, Cardoso MJEDM, Barcia OE. *J Soln Chem* 2009;38:957–81.
- [18] Macdonald SA, Bureau B. *Appl Spect* 2003;57:282–7.
- [19] Heidorn DB, Trehwella J. *Biochemistry* 1988;27:909–15.
- [20] McGeer P. *Ann Physik* 1913;46:809–23.
- [21] Teixeira J. Introduction to small angle neutron scattering applied to colloidal science. In: Chen S-H, Huang JS, Tartaglia P, editors. *Structure and dynamics of strongly interacting colloids and supramolecular aggregates in solution*. Dordrecht: Kluwer; 1982. p. 635–58.
- [22] Kirinčić S, Klofutar C. *Fluid Phase Equilib* 1998;149:233–47.
- [23] Kirinčić S, Klofutar C. *Fluid Phase Equilib* 1999;155:311–25.
- [24] Squires GL. Introduction to the theory of thermal neutron scattering. Dover Edition 1996, Chap. 5. ed. Cambridge: Cambridge University Press; 1978.
- [25] O\_Neil MJ. The merck index. Whitehorse Station, NJ: Merck Research Laboratories; 2006. pp. Entry 7568.
- [26] Pielichowski K, Flejtuch K. *Polym Adv Technol* 2002;13:690–6.
- [27] Becht J, Hellwege KH, Knappe W, Koll. *- Zeit Zeit. Poly* 1967;216-217:150–8.
- [28] Fine RA, Millero FJ. *J Chem Phys* 1973;59(10):5529–36.
- [29] Cleary MP, Chen I-W, Lee S-M. *ASCE J Eng Mech* 1970;106:861–87.
- [30] McGeer S, McCullough RL. *Polym Composites* 1981;2:149–61.
- [31] Lindner J, Vöhringer P, and Schwarzer D. 15th international conference on ultrafast phenomena, OSA Technical Digest Series (CD);2006:TuF1.
- [32] Kolling OW. *J Phys Chem* 1996;100:16087–91.
- [33] Buckingham AD. *Proc Roy Soc Lond Ser A* 1960;255(No 1280):32–9.
- [34] Isogai H, Kato M, Taniguchi Y. *Spectrochim Acta A* 2004;60:3135–9.
- [35] Pinkley LW, Sethna PP, Williams D. *J Opt Soc Am* 1977;67(4):494–9.
- [36] Snyder RG, Maroncelli M, Strauss HL, Hallmark VM. *J Phys Chem* 1986;90:5623–30.
- [37] Zerbi G, Del Zoppo M. *J Chem Soc Farad Trans* 1992;88(13):1835–44.
- [38] Bensebaa F, Ellis TH, Badia A, Lennox RB. *J Vac Sci Technol A* 1995;13:1331–6.
- [39] Banno M, Sato T, Iwata K, Hamaguchi H-O. *Chem Phys Lett* 2005;412:464–9.
- [40] Graener H, Seifert G, Laubereau A. *Chem Phys* 1993;175:193–204.
- [41] Chen W, Sharma M, Resta R, Galli G, Car R. *Phys Rev B* 2008;77. 245114–245114-245114-245115.
- [42] Bonner OD, Curry JD. *Infrared Phys* 1970;10:91–4.
- [43] Kim J, Schmitt UW, Gruetzmacher JA, Voth GA, Scherer NE. *J Chem Phys* 2002;116(2):737–46.
- [44] Heyden M, Bründermann E, Heugen U, Niehues G, Leitner DM, Havenith M. *J Am Chem Soc* 2008;130:5773–9.
- [45] Lappi SE, Smith B, Franzen S. *Spectrochim Acta A* 2004;60:2611–9.
- [46] Segtnan VH, Šašić Š, Isaksson T, Ozaki Y. *Anal Chem* 2001;73:3153–61.
- [47] Huang C, Wikfeldt KT, Tokushima T, Nordlund D, Harada Y, Bergmann U, et al. *Proc Natl Acad Sci U S A* 2009;106:15214–8.
- [48] D\_Arrigo G, Maisano G, Mallamace F, Migliardo P, Wanderling F. *J Chem Phys* 1981;75(9):4264–70.
- [49] Elsaesser T, Kaiser W. *Annu Rev Phys Chem* 1991;42:83–107.
- [50] Elles CG, Crim FF. *Annu Rev Phys Chem* 2006;57:273–302.
- [51] Atkins PW. *Physical chemistry*. New York: Oxford U. Press; 1978.
- [52] Guggenheim EA, McGlashan ML. *Proc Roy Soc Lond A* 1950;203:435–54.
- [53] Kozak JJ, Knight WS, Kauzmann W. *J Chem Phys* 1968;48(2):675–90.
- [54] Matteoli E. *J Phys Chem B* 1997;101:9800–10.
- [55] Shulgin I, Ruckenstein E. *J Phys Chem B* 1999;103:2496–503.
- [56] Rowlinson JS. *Pure Appl Chem* 1993;65:873–82.
- [57] Reichl LE. *A modern course in statistical physics*. Section 8.2. 3rd ed. Weinheim: Wiley-VCH; 2009.
- [58] No KT, Kim SG, Cho K-H, Scheraga HA. *Biophys Chem* 1999;78:127–45.
- [59] Jansson H, Bergman r, Swenson J. *Phys Rev Lett* 2010;104. 017802–017801-017802-017804.
- [60] Debye P. English translation of Ann. Physik. 1915 paper. The collected papers of Peter J. W. Debye. New York: Interscience; 1954.
- [61] Derjaguin BV, Bazaron UB, Lamazhapova KD, Tsidypov BD. *Phys Rev A* 1990;42:2255–8.
- [62] Noirez L, Baroni P, Mendil-Jakani H. *Polym Int* 2009;58:962–8.
- [63] Noirez L, Baroni P. *J Mol Struct* 2010;972:16–21.
- [64] Bieze TWN, van der Maarel JRC, Eisenbach CD, Leyte JC. *Macromolecules* 1994;27:1355–66.
- [65] Derkaoui N, Said S, Grohens Y, Olier R, Privat M. *J Coll Interface Sci* 2007;305:330–8.
- [66] Polverari M, van de Ven TGM. *J Phys Chem* 1996;100:13687–95.
- [67] Jeffery S, Hoffmann PM, Pethica JB, Ramanujan C, Özer Ö, Oral A. *Phys Rev B* 2004;70. 054114–054111-054114-054118.

- [68] Bieze TWN, Barnes AC, Huige CJM, Enderby JE, Leyte JC. *J Phys Chem* 1994;98: 6568–76.
- [69] Leikin S, Rau DC, Parsegian VA. *Proc Natl Acad Sci U S A* 1994;91:276–80.
- [70] Soper AK. *J Phys Condens Matter* 2007;19:335206.
- [71] Filfil R, Chalikian TV. *J Mol Biol* 2003;326:1271–12288.
- [72] Pashley RM, Kitchener JA. *J Coll Interface Sci* 1979;71(3):491–500.
- [73] Zheng J-M, Chin W-C, Khijniak E, Khijniak Jr E, Pollack GH. *Adv Coll Interface Sci* 2006;127:19–27.
- [74] Shelton DP. *J Chem Phys* 2012;136:044503.
- [75] Fameau A-L, Cousin F, Navailles L, Nallet F, Boué F, Douliez J-P. *J Phys Chem B* 2011;115:9033–9.
- [76] Neilson GW, Skipper N. *Chem Phys Lett* 1985;114:35–8.
- [77] Bowron DT, Soper AK, Finney JL. *J Chem Phys* 2001;114(14):6203–18.
- [78] Ebbinghaus S, Kim SJ, Heyden M, Yu X, Huegen U, Gruebele M, et al. *Proc Natl Acad Sci USA* 2007;104(52):20749–52.
- [79] Assarsson PG, Leung PS, Safford GJ. *ACS Polym Preprints* 1969;10(2):1241–7.
- [80] Dissanayake MAKL, Frech R. *Macromol* 1995;28:5312–9.
- [81] Matsuura H, Fukuhara K. *J Mol Struct* 1985;126:251–60.
- [82] Wang RY, Himmelhaus M, Fick J, Herrwerth S, Eck W, Grunze M. *J Chem Phys* 2005;122. 164702-164701–164702-164706.
- [83] Yoshihara T, Tadokoro H, Murahashi S. *J Chem Phys* 1964;42(9):2902–11.
- [84] Miyazawa T, Fukushima K, Ideguchi Y. *J Chem Phys* 1962;37:2764–76.
- [85] Koenig JL, Angood AC. *J Poly Sci A-2* 1970;8:1787–96.
- [86] Glinka CJ, Barker JG, Hammouda B, Krueger S, Moyer JJ, Orts WJ. *J Appl Cryst* 1998;31(3):430–45.
- [87] Kline SR. *J. Appl. Cryst* 2006;39:895–900.